*Minerals* **2012**, *2*, 318-337; doi:10.3390/min2040318

OPEN ACCESS

*minerals*

**ISSN 2075-163X**
www.mdpi.com/journal/minerals

*Article*

# Major- and Trace-Element Compositions of Indicator Minerals that Occur as Macro- and Megacrysts, and of Xenoliths, from Kimberlites in Northeastern Angola

**Sandra E. Robles-Cruz [1,*], Joan Carles Melgarejo [1], Salvador Galí [1] and Monica Escayola [2]**

[1] Department of Crystallography, Mineralogy and Mineral Deposits, University of Barcelona, Barcelona 08028, Spain; E-Mails: joan.carles.melgarejo.draper@ub.edu (J.C.M.); gali@ub.edu (S.G.)

[2] CONICET-IDEAN Institute of Andean Studies, Andean Tectonic Laboratory, University of Buenos Aires, Buenos Aires C1033AAJ, Argentina; E-Mail: m_escayola@hotmail.com

***** Author to whom correspondence should be addressed; E-Mails: sandra_robles@ub.edu or sandrarobc@gmail.com; Tel.: +506-883-939-81; Fax: +506-224-244-11.

*Received: 30 August 2012; in revised form: 22 September 2012 / Accepted: 28 September 2012 / Published: 26 October 2012*

---

**Abstract:** In this study, we compare the major- and trace-element compositions of olivine, garnet, and clinopyroxene that occur as single crystals (142 grains), with those derived from xenoliths (51 samples) from six kimberlites in the Lucapa area, northeastern Angola: Tchiuzo, Anomaly 116, Catoca, Alto Cuilo-4, Alto Cuilo-63 and Cucumbi-79. The samples were analyzed using electron probe microanalysis (EPMA) and laser-ablation inductively coupled plasma-mass spectrometry (LA-ICP-MS). The results suggest different paragenetic associations for these kimberlites in the Lucapa area. Compositional overlap in some of the macrocryst and mantle xenolith samples indicates a xenocrystic origin for some of those macrocrysts. The presence of mantle xenocrysts suggests the possibility of finding diamond. Geothermobarometric calculations were carried out using EPMA data from xenoliths by applying the program PTEXL.XLT. Additional well calibrated single-clinopyroxene thermobarometric calculations were also applied. Results indicate the underlying mantle experienced different equilibration conditions. Subsequent metasomatic enrichment events also support a hypothesis of different sources for the kimberlites. These findings contribute to a better understanding of the petrogenetic evolution of the kimberlites in northeastern Angola and have important implications for diamond exploration.

**Keywords:** Angola; kimberlite; olivine; garnet; clinopyroxene; diamond; thermobarometry; mantle xenoliths; REE; Sm/Nd isotopes

## 1. Introduction

In Angola, more than 700 occurrences of kimberlite are distributed on a trend northeast to southwest from Lunda Sul and Lunda Norte, up through Huambo, Benguela, and Huila provinces. Diamond was first reported in Angola in 1590 [1]. In 1952, the first kimberlite in Angola, Camafuca-Kamazambo, was discovered [2]. Since then, and especially after thirty years of civil war, Angola has become known as an important diamond producer. The Catoca kimberlite in Lunda Sul province, the first kimberlite mine in Angola, was for a long time the only kimberlite under production. In 2007, two more pipes came on line, and subsequently other exploration projects have started in the country. By 2010, the Catoca kimberlite had produced over 8.36 million carats, valued at US$ 976 million [3].

There are several diamondiferous and barren kimberlites in the northeastern area. However, there are no detailed studies that allow a full understanding of their relationship with the underlying mantle, or their spatial distribution. Six kimberlites from northeastern Angola will be considered for this study. They range from poor to very high level of diamond production: Alto Cuilo 4 (AC4), Cucumbi-79 (CU79), Alto Cuilo-63 (AC63), Anomaly 1116 (An116), Tchiuzo (TZ) and Catoca (CA). These kimberlites are located in the Lucapa area and emplaced in Archean metamorphic rocks, in the Kassai-Congo Craton.

Kimberlites are volatile-rich potassic ultrabasic rocks usually with an inequigranular texture as a result of the presence of crystals, compound clasts, and interstitial matrix [4,5]. Crystals can be: megacrysts, crystals of more than 1.0 cm at maximum dimension (MD); macrocrysts, crystals between 0.5 and 10 mm at MD; or microcrysts, crystals less than 0.5 mm at MD. Xenoliths are rare; in these kimberlites, most of them consist of metasomatized peridotite and phlogopite-rich suites.

The aim of this paper is to establish the major- and trace-element compositions of indicator minerals: olivine, garnet, and clinopyroxene, that occur as single crystals with those derived from xenoliths from six kimberlites from the Lucapa area, northeastern Angola: TZ, An116, CA, AC4, AC63 and CU79. This area is where most of the diamondiferous kimberlites identified so far are concentrated. We estimate reliable conditions of pressure and temperature for selected samples. Also we have measured Sm/Nd isotopes from the rare xenoliths to better understand their petrogenesis.

## 2. Geological Setting

The exposed rocks in Angola range from Archean age to Recent (Figure 1). This geological history may be divided in three main stages [6,7]: (1) The Archean orogeny is recorded by the Central Shield, Cuango Shield and Lunda Shield, mainly composed of gabbro, norite and charnockitic complexes, which constitute the Angolan basement. (2) There are three main Proterozoic cycles (Eburnean in the Paleoproterozoic, Kibaran in the Mesoproterozoic, and Pan-African in the Neoproterozoic), of which the Eburnean is the most important and characterized by complex volcanosedimentary rocks, gneisses, migmatites, granites and syenites. This regional Paleoproterozoic event was followed by the Kibaran

cycle, which was related to extensional events along the border of the Congo craton where later clastic-carbonatic sequences and local basic magmatism took place. The Pan-African orogeny was associated with the development of Gondwana and led to the generation of fold belts and granitic intrusions. (3) Phanerozoic sequences covered the older rocks as events associated with the formation of Pangea and the consecutive break-up of Gondwana which contributed to the formation of rift basins associated with deep fault systems and later intraplate magmatism (alkaline, carbonatitic, kimberlitic) and marginal basins.

**Figure 1.** Geological setting of the northeastern Angola kimberlites of this study (after Perevalov *et al*. [8], Giraud *et al*. [7], Egorov *et al*. [9]).

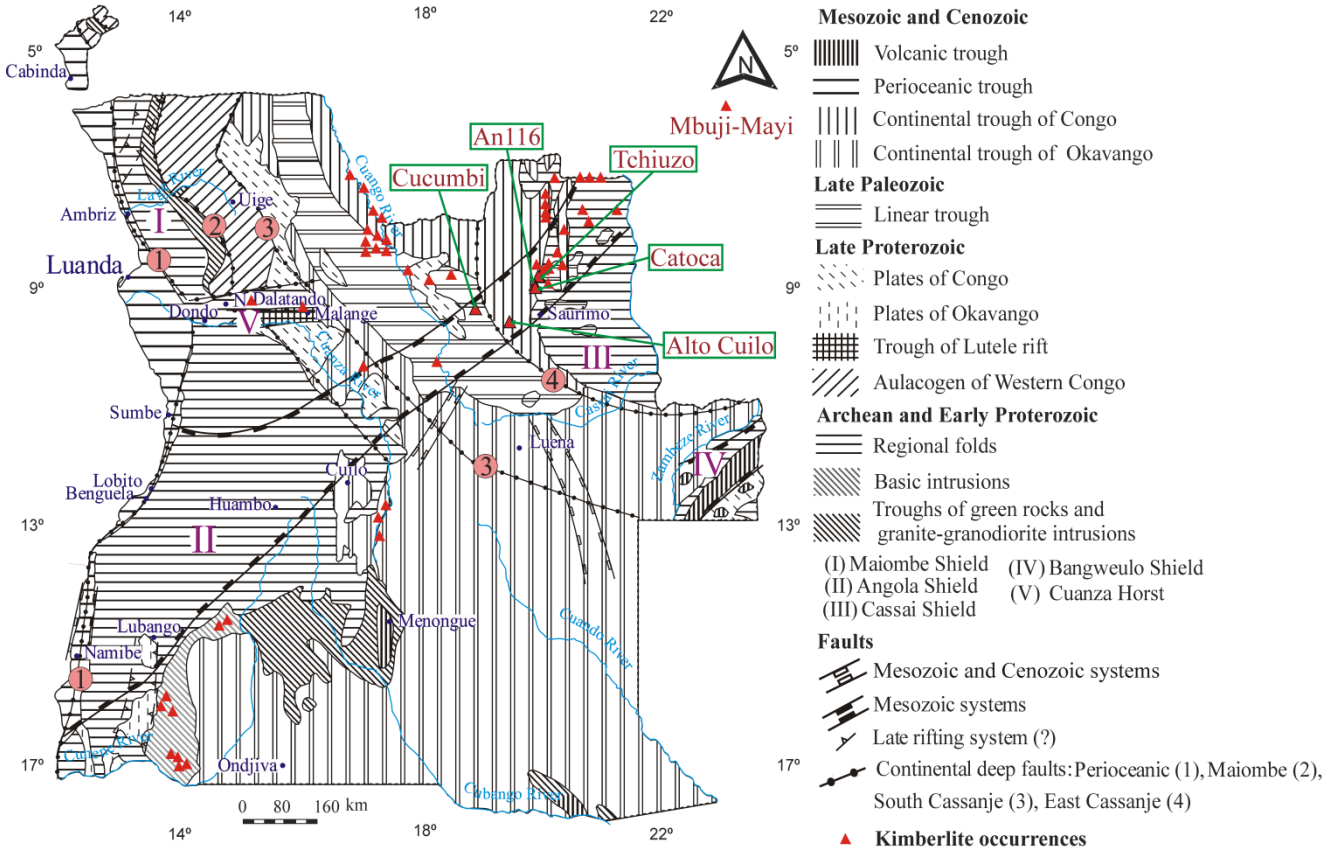


The Lower Cretaceous regional extension caused the development of deep faults and grabens with NE-SW and NW-SE trends. The Lucapa structure, a deep-seated fault system, corresponds to the first group, and the northeastern part is the focus of most of the diamondiferous kimberlites in Angola, whereas the southwestern zone comprises important outcrops of undersaturated alkaline rocks and carbonatites [2]. Other minor kimberlite fields are found in southwestern Angola [9]. This geological configuration sets a tectonic control on the presence of some of the kimberlites in northeastern Angola. The emplacement of the Catoca kimberlite (middle of Aptian and Albian) has been recently correlated with these regional tectonic events [10]. Kimberlite emplacement ages in the Alto Cuilo range between 145.0 ± 4.0 ($^{206}Pb/^{238}U$ for perovskite) and 113.0 ± 0.8 Ma ($^{206}Pb/^{238}U$ for zircon) [11]. Synsedimentary continental sediments associated with the filling of the Lucapa structure (Calonda Formation) can also contain diamond crystals in paleoplacers; alluvial diamond is found in placers associated with rivers draining these diamondiferous areas.

## 3. Analytical Techniques

Six hundred and fifty samples were studied with an optical petrographic microscope. Then representative samples of mantle xenoliths (51 samples), mega- (3 grains), macro- (116 grains), and microcrysts (23 grains) of olivine, garnet, and clinopyroxene were examined by back-scattered electron (BSE) images using SEM-ESEM with EDS microanalysis and electron-probe microanalysis (EPMA). More than 800 microprobe analyses were carried out to obtain the mineral chemistry of major elements. The major elements were analyzed using a JXA JEOL-8900L EPMA at the Department of Earth and Planetary Sciences, McGill University (Montreal, Quebec), using the ZAF correction method. Acceleration voltage was 20 kV, beam current 20 nA, and beam diameter 5 μm. The counting time for most elements was 20 s on peaks and 20 s on the background. Standardized natural and synthetic minerals were used for calibration.

Then 14 representative samples of xenoliths and 25 macrocrysts of garnet, clinopyroxene, and olivine were selected to perform trace-element analyses using laser-ablation inductively coupled plasma mass spectrometry (LA-ICP-MS) at the Geological Survey of Canada, Ottawa. The data were acquired with a Photon-Machines Analyte 193 nm Excimer laser ablation in combination with an Agilent 7500cx quadrupole ICP-MS, a powerful technique for reliable solid analysis of samples. Data reduction was performed with the GLITTER 4.4.2 software. The primary calibration standard was the synthetic glass standard of the 610 series (NIST SRM 610) of the National Institute of Standards and Technology, using $SiO_2$ for internal standardization. The GSE-1G (a synthetic reference glass with basaltic major-element composition and trace elements abundance of *ca.* 500 μg/g) was used as a secondary standard.

Finally, accurate high-precision Sm/Nd isotopic compositions of eight samples of xenoliths (1.5 to 7 cm in diameter) from kimberlites CA, CU79, and CU80 (for comparison purposes) were carried out at the Pacific Centre for Isotopic and Geochemical Research (PCIGR) at the University of British Columbia, using a Thermo Finnigan Triton thermo-ionization mass spectrometer (TIMS). We used the analytical procedures for sample dissolution, ion exchange, and leaching described by Weis *et al.* [12]. The normalization procedure has been applied to the Nd isotopic ratios using La Jolla Nd as the reference material (measured ratio normalized to La Jolla $^{143}Nd/^{144}Nd = 0.511858$).

## 4. Morphology of the Kimberlite Pipes Studied in Northeastern Angola

The CA, TZ, An116, AC4, AC63 and CU79 kimberlites are located within the Kasai craton (Figure 1). The pipes generally appear in clusters along a network of local fractures. They are of variable shape and dimension, some very large up to 900 m in diameter (*i.e.*, Catoca). Some pipes in this area are diamondiferous, and do have an economic grade. Crater and diatreme facies can be recognized despite the intense weathering affecting kimberlites up to a depth of 150–200 m. Because of the weathering the number of fresh xenoliths and crystals is limited, and conditioned the selection of samples for this study. Next to olivine, serpentine is the most abundant mineral in the studied kimberlites, followed by calcite in the CA, TZ, An116, and AC. Phlogopite is the second most abundant mineral in the Cucumbi cluster.

### *4.1. TZ, An116 and CA Kimberlites*

The CA kimberlite has a circular shape on the surface. This pipe exhibits crater and diatreme facies. For this study, we analyzed samples to a maximum of 609 m depth. A new exploration project taking samples to a depth of 800 m started in 2010 [13]. Crater facies are found up to 270 m in depth, and are composed of epiclastic sandstones, coarse debris rimming the crater, and a higher concentration of volcaniclastic material at a lower depth of the crater [14]. Quartz (without a reaction rim) and K-feldspar are the most abundant minerals in the volcaniclastic rocks (VR). Altered crystals of garnet, diopside, and rare ilmenite may be present. The diatreme facies rocks, which are more than 700 m thickness, are composed of volcaniclastic kimberlite (VK) and volcaniclastic kimberlite breccias (VKB), with tuffisitic kimberlite (TK) in the deepest zone. There are abundant olivine macrocrysts completely replaced by serpentine and secondary carbonates. Macrocrysts of clinopyroxene, garnet, ilmenite (Fe-rich, Mg-rich, and Mn-rich ilmenite), chromite, magnetite, zircon, phlogopite, hematite, and amphibole also are present. Orthopyroxene has been identified, but is completely replaced by bastite lizardite. The diatreme facies rocks are strongly altered all along the profile. Abundant xenoliths derived from the host rocks are present, (e.g., gneiss, amphibolite, and granite); some carbonatite xenoliths which could be present in the crust or beneath the kimberlite volcano; mantle-derived xenoliths (*i.e.*, garnet lherzolites, phlogopite-garnet wehrlite, and very rare eclogite) are sparse and have been intensively altered. The groundmass contains lizardite, smectite, apatite, calcite, ilmenite and chromite. Titanite, zirconolite, baddeleyite, barite, dolomite, witherite, barytocalcite, strontianite, sulfides, and minor minerals are also widespread in the matrix.

The TZ kimberlite is characterized by the presence of crater and diatreme facies. The first 30 m contains VR composed of quartz, hematite, K-feldspar, plagioclase, amphibole, and spinel. Diatreme-facies rocks are composed of VK and VKB with macrocrysts of replaced olivine and orthopyroxene, garnet, clinopyroxene, spinel (in some cases in a "necklace" shape around pellets of serpentine), apatite, ilmenite, amphibole, phlogopite (some of them with inclusions of ilmenite), and zircon in a groundmass of lizardite, smectite, apatite, calcite, ilmenite and chromite. Xenoliths from amphibolites are very common. Mantle xenoliths are very rare, *i.e.*, garnet lherzolite and carbonatite; and usually altered. This pipe was drilled up to 310 m in depth.

The An116 pipe is located on a magnetic anomaly close to the Catoca area, and samples were taken down to a depth of 88 m. These samples describe VR, mainly PK, in which quartz and microcline are the most abundant minerals, and "mafic" xenoliths of ilmenite-calcite-phlogopite are present in the first 10 m. Samples from 10 to 88 m in depth returned VK facies composed of macrocrysts of ilmenite, altered clinopyroxene, phlogopite, hematite, and plagioclase, mafic xenoliths (amphibolites) and metasomatized mantle-derived xenoliths *i.e.*, phlogopite-ilmenite-clinopyroxene suites (PIC suites), altered metasomatic peridotites.

### *4.2. The AC4 and AC63 Kimberlites*

The AC4 and AC63 pipes are also covered for the first 50 and 100 m, respectively, by sandstone, litharenite, and arkose from the Calonda Formation, Kalahari Group, and Quaternary deposits, as has been observed in most of the kimberlites in the Alto Cuilo cluster [15]. These kimberlites exhibit

crater- and diatreme-facies rocks. The crater-facies rocks are mainly composed of VR, mainly pyroclastic rocks (PR) and resedimented volcaniclastic kimberlites (RSVK). Macrocrysts of clinopyroxene, hematite, mica, microcline, and ilmenite are present in the microlitic matrix, which contains clinopyroxene, mica, microcline, ilmenite, and higher content of hematite. The diatreme facies rocks contain VKB composed of macrocrysts of clinopyroxene, garnet, ilmenite with homogeneous and symplectitic textures, phlogopite and rare xenoliths of phlogopite-garnet wehrlite and altered phlogopite peridotites. Mantle xenoliths have not been found in the AC4 pipe. The groundmass is composed of serpentine, calcite, and hematite.

### *4.3. The CU79 Kimberlite*

The CU79 kimberlite exhibits two facies: crater and diatreme. The first 50 m of the crater facies contains VR with ferruginous cement, interbedded with layers of lapilli. The facies then changes to TK, which is generally massive, poorly sorted, and clast-supported, and is present as far down as 200 m. The macro- and microcrysts are composed of anhedral olivine replaced by serpentine and smectite, garnet, ilmenite, clinopyroxene, and phlogopite. Some of these crystals are enclosed in a pelletal assemblage of serpentine, but all the crystals have a chaotic distribution in the matrix. The matrix is an interclast groundmass of serpentine, microcrystals of phlogopite, less common chlorite, smectite and calcite [16]. The ilmenite texture is usually either cumulus or homogeneous. Mg-rich ilmenite (9–13 wt % MgO) is present as rounded mega- and macrocrysts, as part of xenoliths, and as inclusions in phlogopite. In some cases, macrocrysts of ilmenite are partially replaced along the borders by perovskite and spinel. Garnet and clinopyroxene are usually present as mega- and macrocrysts, and rarely as part of xenoliths. This kimberlite rarely has mantle xenoliths *i.e.*, garnet lherzolite, phlogopite-garnet wehrlite, and relatively abundant phlogopite-rich (olivine poor or absent, without garnet [17]) xenoliths.

## 5. Major-Element Composition

The kimberlites in this suite exhibit differences in their composition and abundance of olivine, garnet, and clinopyroxene depending on the location and type of kimberlite.

### *5.1. Olivine*

Olivine is abundant in the TZ, CA, and An1116 kimberlites, forming up to 65% volume of the total mineral components. However, fresh olivine has only been found in the CA kimberlite. The grains generally occur as macrocrysts (most of them anhedral) and microcrysts (subhedral to anhedral), dark and light green to pale greenish white, depending on the degree of alteration. Most of the grains (approximately 95%) are replaced by lizardite, with other alteration minerals *i.e.*, calcite, smectite, chlorite, magnetite, and sulfides. Olivine macrocrysts from the CA kimberlite (Figure 2) occur as: (1) homogeneous crystals; (2) crystals rimmed by “iddingsite”; (3) zoned macrocrystals. The first population (Table 1, supplementary file) has an average composition of $Fo_{92}$ and extremely low average values for CaO (0.01 wt %), and MnO (0.11 wt %). The second population also has an average composition of $Fo_{92}$, CaO (0.01 wt %), and MnO (0.13 wt %). The third population of crystals exhibits

zonation with an average composition of core $Fo_{90}$, middle $Fo_{87}$, and rim $Fo_{85}$. The average values varying from core to rim are: CaO (0.02–0.04 wt %), MnO (0.13–0.19 wt %), $Cr_2O_3$ (0.01–0.06 wt %), $TiO_2$ (0.01–0.03 wt %) and NiO (0.36–0.13 wt %). Olivine macrocryst compositions are very similar to archetypal cratonic peridotites, which has a mean Mg# of 92.6 and indicates melt depletion [18].

**Figure 2.** CaO *vs.* Mg# diagram for olivine macrocrysts from the CA kimberlite. Error bars indicate standard deviation of CaO (wt %).

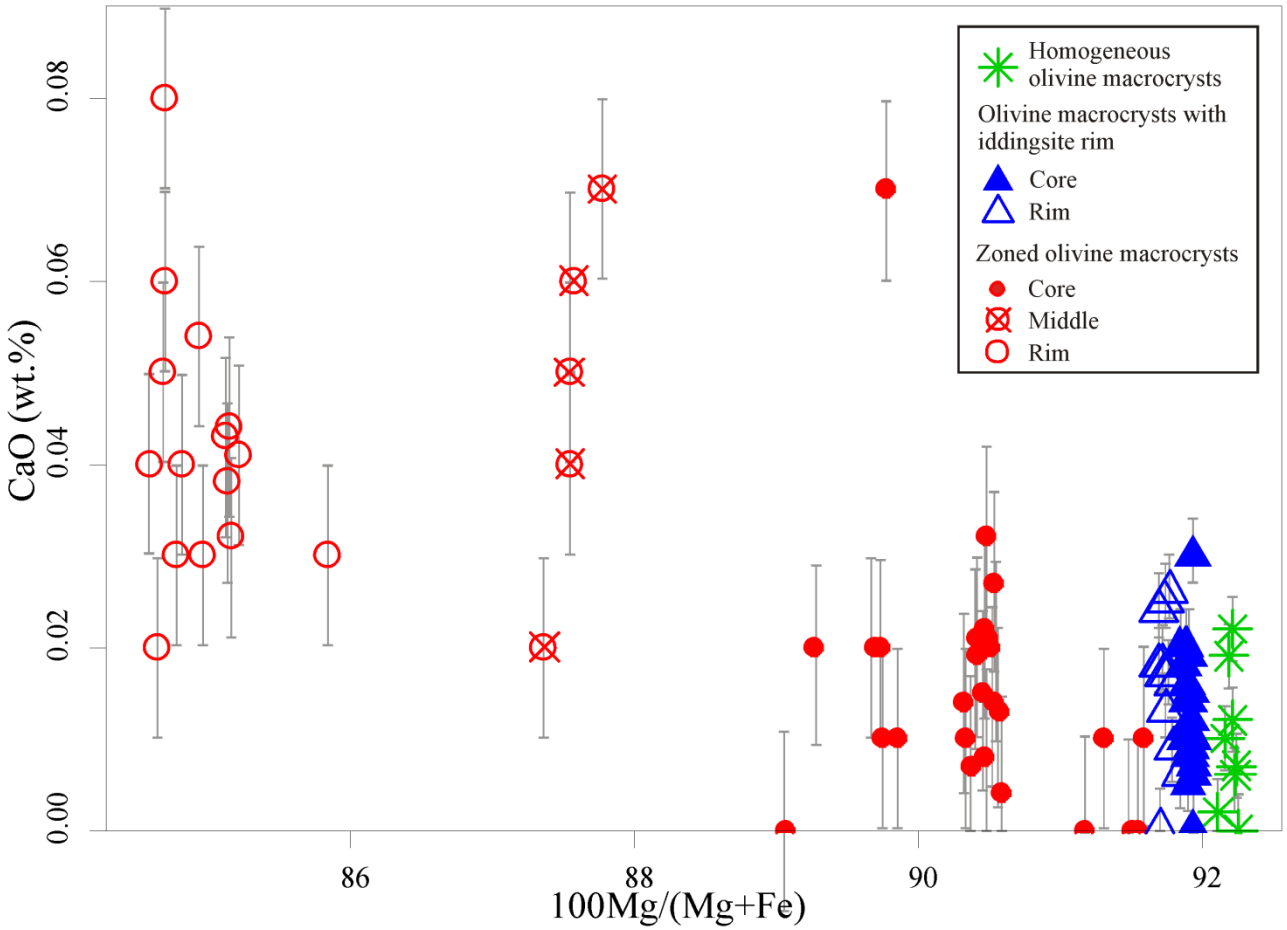


*5.2. Garnet as Macrocrysts and within Xenoliths*

The CA and TZ kimberlite includes dark pink to dark orange anhedral macrocrysts garnet (G9 and G10 after Grütter *et al.* [19], Figure 3). Some of the garnet macrocrysts are partially altered to chlorite, or replaced by hematite and calcite along fractures. Garnet (Table 2, supplementary file) is also present in eclogite (CA), garnet lherzolite with and without ilmenite (CA, TZ), and phlogopite-garnet wehrlite with and without ilmenite (CA) xenoliths. Garnet macrocrysts from the CU79 kimberlite are mainly pink to orange (G9). Few garnet grains are among the microcrysts. Garnet is also found in garnet lherzolite, garnet-phlogopite wehrlite xenoliths from CU79, and bimineralic associations of G9-diopside. The garnet from AC kimberlite is usually found as a microcryst (AC4) or in garnet-phlogopite wehrlite xenoliths (AC63). Garnet from CA, TZ, AC63, and CU79 fall in the mantle-derived field (Figure 4), whereas garnet that has been found so far in the AC4 pipe indicates a crust- derived origin.

**Figure 3.** $Cr_2O_3$ *vs.* CaO diagram for garnet with superimposed isobars according to the P38 barometer calculation [19]. Graphite-diamond constraint (GDC).

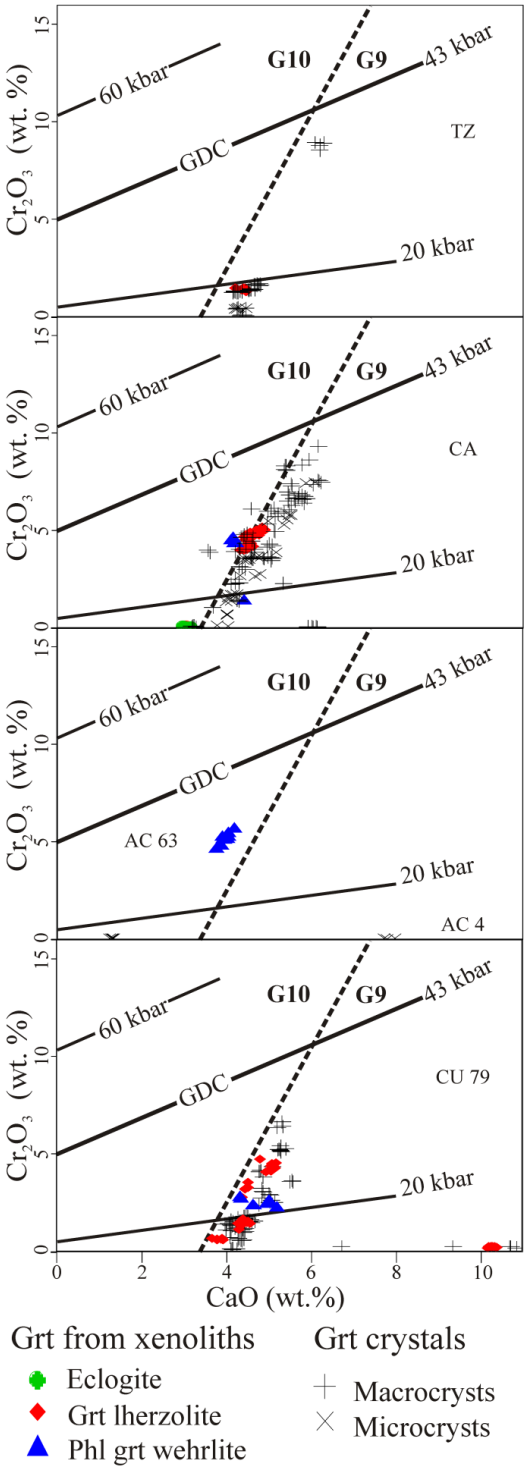

**Figure 4.** Ca# *vs.* Mg# for garnet from the (**a**) TZ; (**b**) CA; (**c**) AC63, AC4; (**d**) CU79 kimberlites.

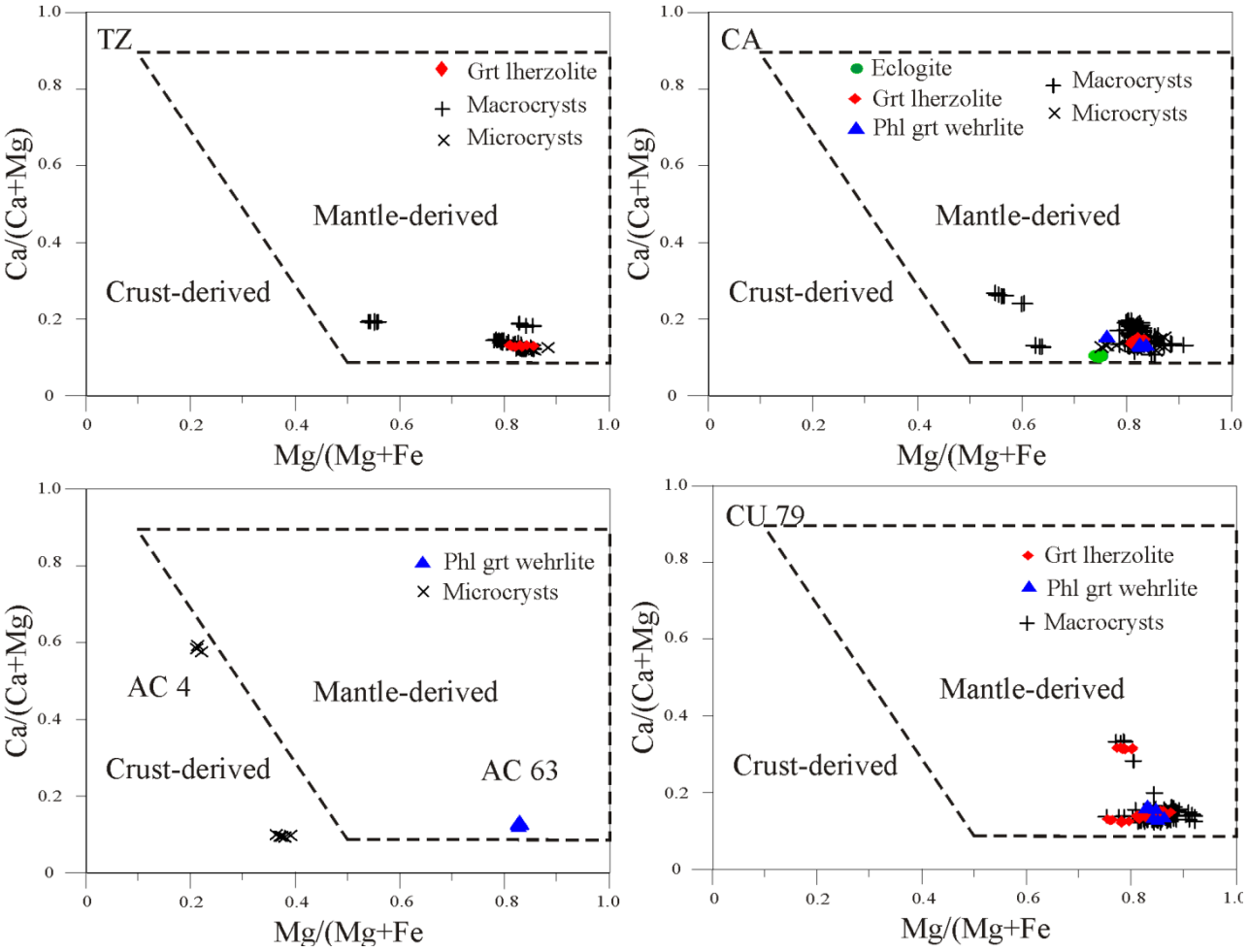


*5.3. Clinopyroxene Mega- and Macrocrysts and in Xenoliths*

Three populations of clinopyroxene can be identified on the basis of an Al-Cr-Na plot (Figure 5): (1) Clinopyroxene in a lherzolitic association; (2) Low-Cr clinopyroxene that plots between Al and Na extremes; (3) Low-Na clinopyroxene. Clinopyroxene in a lherzolitic association has been found in all the kimberlites studied with slight variations in the Cr content between pipes (Table 3, supplementary file). Cr-rich diopside is relatively common in the CA pipe, and shows the highest concentrations in Cr. Low-Cr clinopyroxene was found in the CA, some in the TZ, and the CU79 pipes. Low-Na clinopyroxene is present in the CA pipe with a relatively high content of Cr, whereas low-Na and low-Cr clinopyroxene is found in the TZ and the CU79 pipes. All the clinopyroxene falls in the "on craton" field, except for a clinopyroxene inclusion in garnet from CU79 (Figure 6).

**Figure 5.** Plot of Al-Cr-Na (apfu) for clinopyroxene from the kimberlites studied.

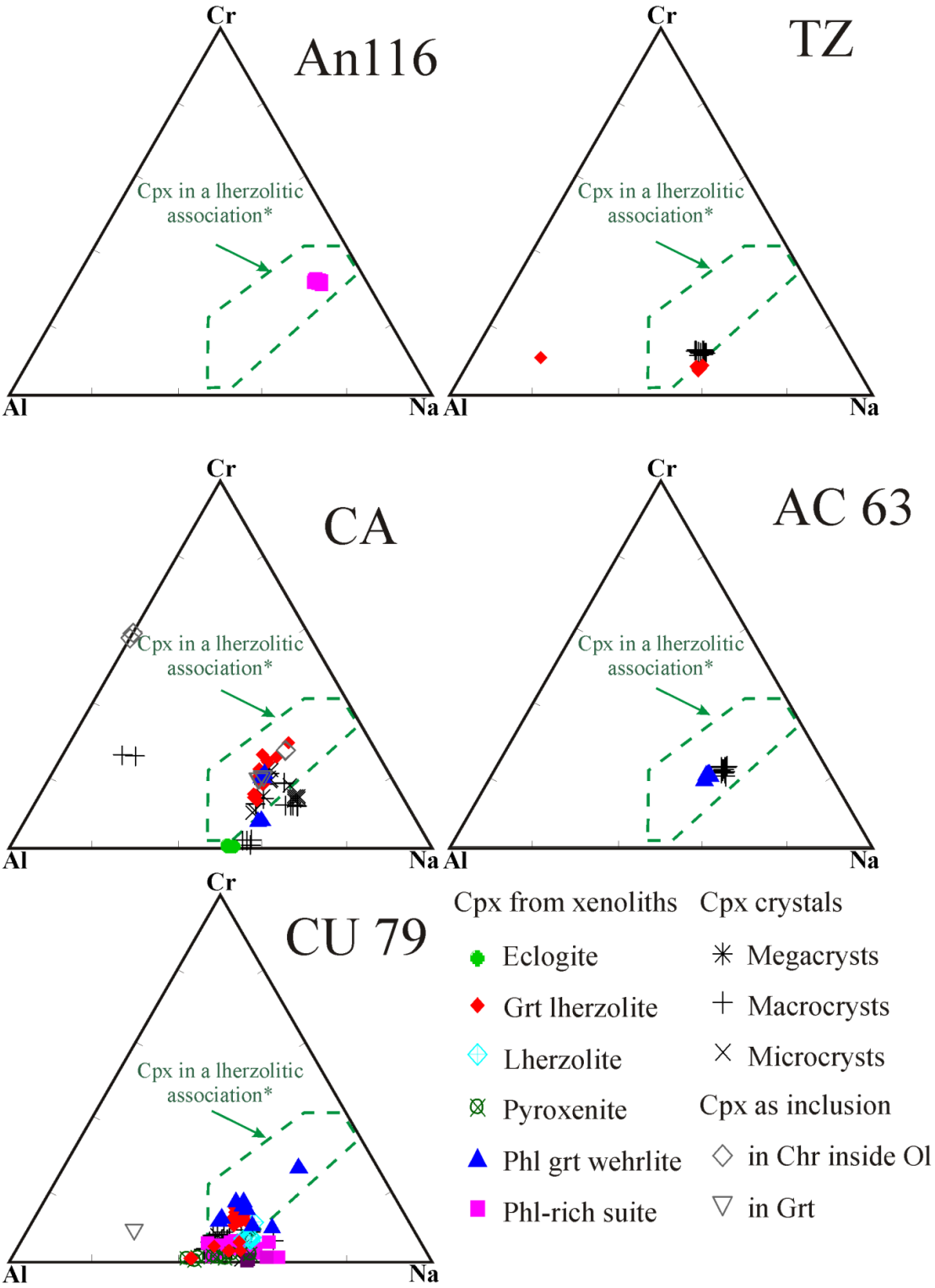


Notes: * After Morris *et al.* [20].

**Figure 6.** $Cr_2O_3$ *vs.* $Al_2O_3$ diagram for clinopyroxene from the (**a**) An116, TZ; (**b**) CA; (**c**) AC63; (**d**) CU79 kimberlites. Classification diagram after Ramsey [21].

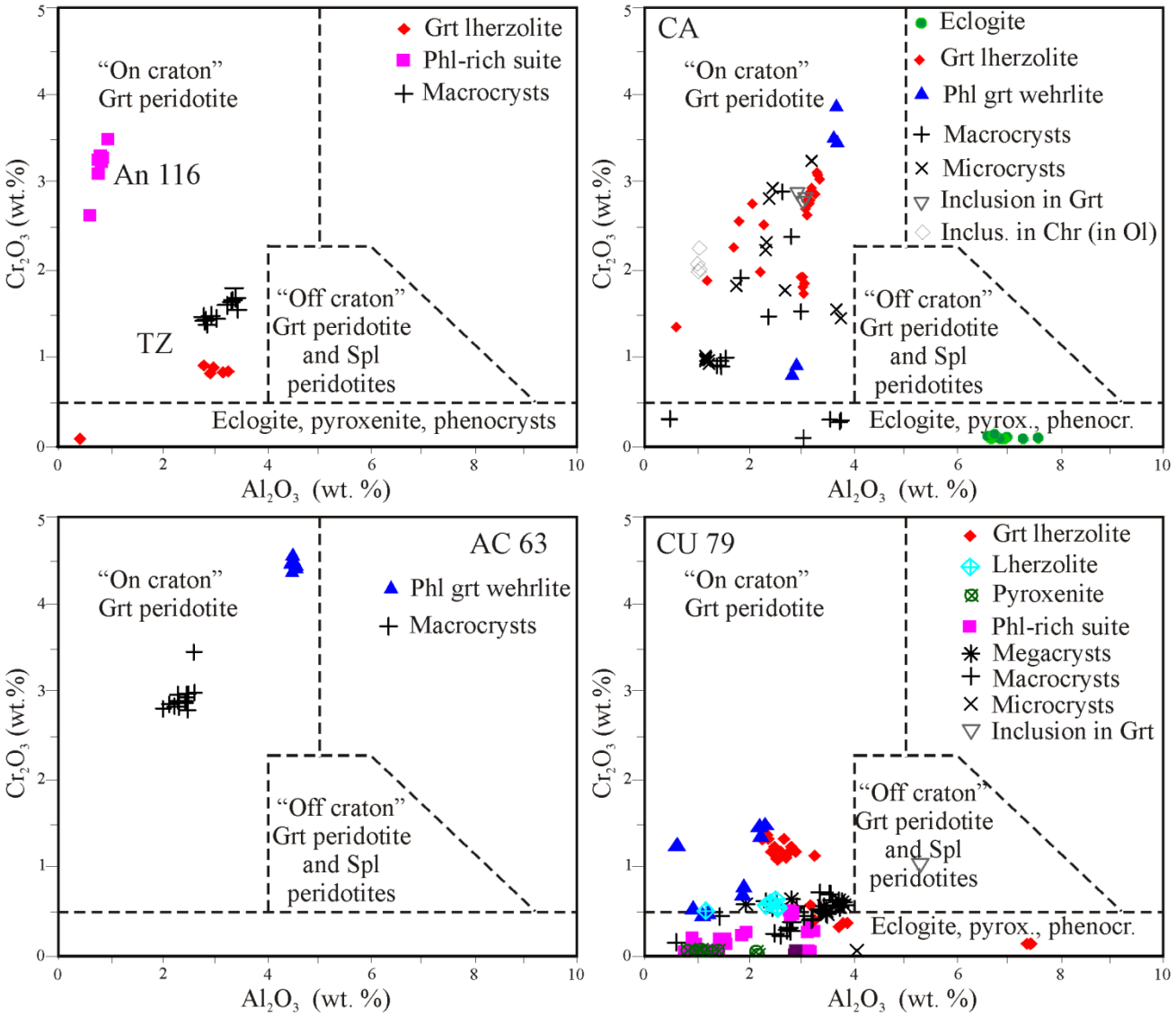


## 6. Geothermobarometry

Comparison and evaluation of results obtained from different pressure and temperature (PT) combinations were carried out. The thermobarometer combination used is based on element-exchange reactions between clinopyroxene and garnet that are believed to be in equilibrium (xenoliths), which provides better evaluation of PT results than calculations based on single crystals. First, we selected only the most representative fresh xenoliths from the CA, TZ, CU79, and AC63 kimberlites, then we proceeded to calculate P and T on the basis of EPMA data and by obtaining the average composition for each mineral from each xenolith (*i.e.*, only one average value-point for each type of xenolith). We used the program PTEXL.XLT, prepared by T. Stachel [22]. The well-calibrated single-clinopyroxene thermobaromether of Nimis and Taylor [23] also was applied, in order to compare values of both T and P, which yielded reliable temperature estimates compared to the T-P results obtained from thermobarometry of xenoliths. We used the following calibration for the single-clinopyroxene thermobaromether: (1) clinopyroxene that falls in the garnet peridotite field "on-craton" defined by

Ramsay [21] in the diagram $Cr_2O_3$ *vs.* $Al_2O_3$ (Figure 6); (2) clinopyroxene above the field of Low-Al peridotite (Figure 7).

**Figure 7.** $Al_2O_3$ *vs.* MgO diagram for discrimination of no Low-Al peridotite clinopyroxene type for the geothermobarometric calculations based on of single crystals of clinopyroxene (after Nimis [24]).

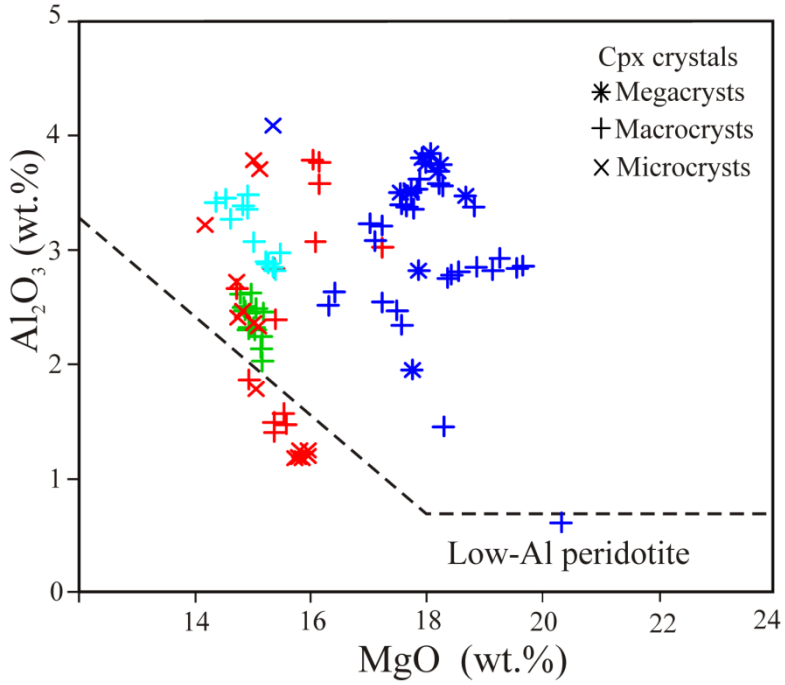


Calculated temperature and pressure from xenoliths is less scatter than T-P data calculated from single crystals (Figure 8). However, most of the data fall within error of estimate. The calculated northeastern Angola paleogeotherm fit a single value for the CA and the CU79 kimberlites. Only one phlogopite-garnet lherzolite xenolith from the AC63 kimberlite was able to be used and plotted in the same paleogetherm than the CA and CU79 kimberlites. The differences in T-P values between these kimberlites may reflect the different way each kimberlite sampled the lithosphere. The lithospheric thickness calculated from the northeastern Angola paleogeotherm yielded 192 km. A quantitative comparison between Angola lithosphere and reference geotherms in southern Africa (Bultfontein and Finsch kimberlites, after Mather *et al.* [25]), indicates a slightly cooler (steeper) paleogetherm for Angola than the paleogetherms calculated from southern Africa.

**Figure 8.** Pressure and temperature values calculated for xenoliths using the equation Nimis and Taylor [23] (NT2000): Garnet lherzolite (diamonds) and phlogopite garnet wehrlite (triangles); and for single clinopyroxene macrocrysts (cross) from the TZ (purple), CA (red), AC63 (green) and CU79 (blue) kimberlites. Paleogeotherm calculated using FITPLOT program (blue line, with pink and purple lines representing the error envelope). P-T data calculated from mantle xenoliths from the Bultfontein kimberlite (dark gray shading) and paleogeotherm (dark gray dashed line); and P-T data calculated from mantle xenoliths from the Finsch kimberlite (light gray shading) and paleogeotherm (light gray point line) after Mather *et al.* [25].

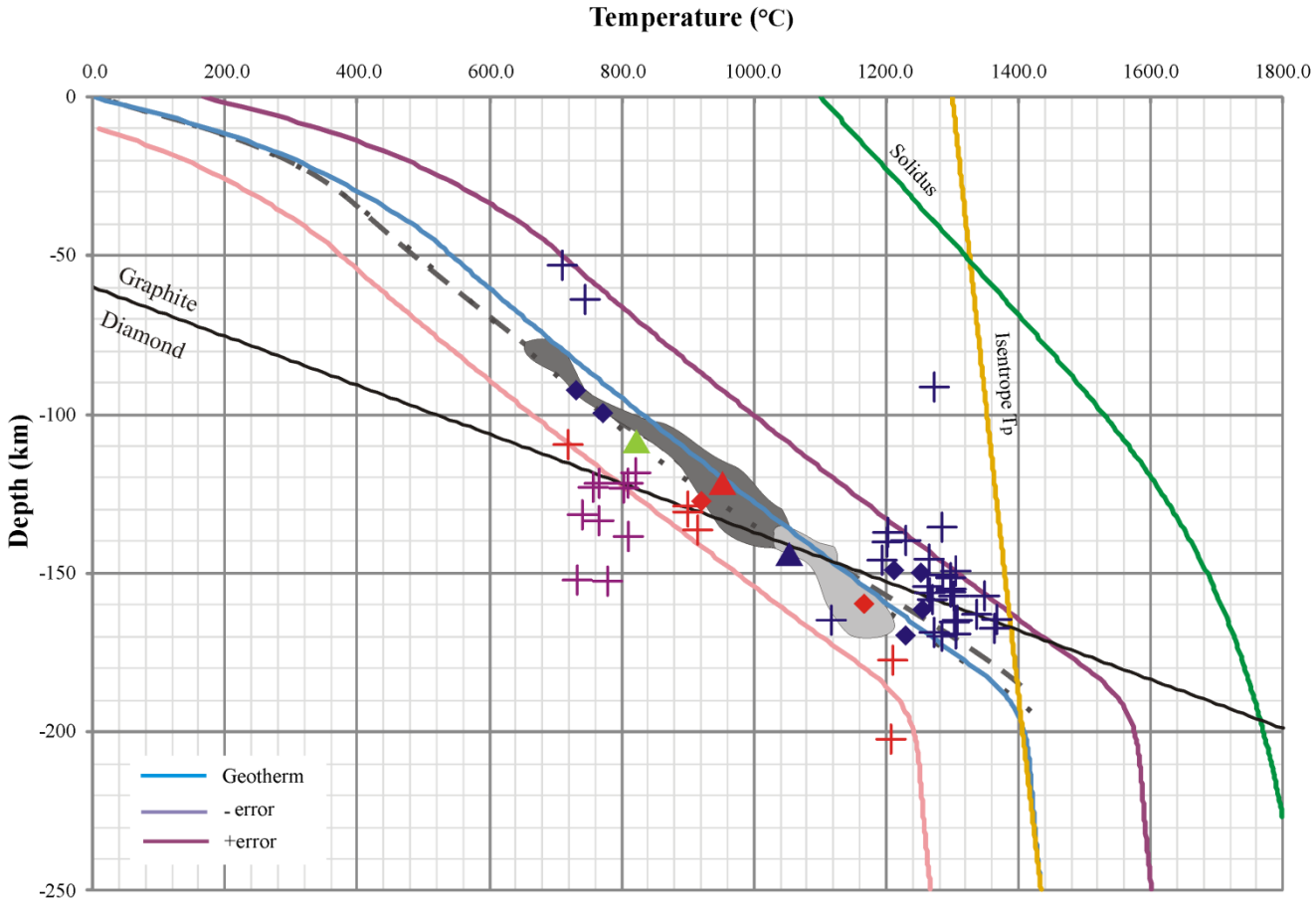


## 7. Trace-Element Chemistry

About one hundred sixty trace-element analyses were performed on garnet and clinopyroxene from representative macrocrysts (about 80 grains) and mantle xenoliths (14 xenoliths) from the CA, TZ and CU79 kimberlites (Table 4, supplementary file). Three main different trends for garnet can be identified in the Catoca kimberlite on the basis of chondrite-normalized Rare Earth Element patterns ($REE_N$) (Figure 9). (1) Garnet of eclogitic affinity with "normal" [26] $REE_N$ patterns, and slightly enriched in Light Rare Earth Element (LREE). (2) Garnet from garnet lherzolite and phlogopite-garnet wehrlite xenoliths can exhibit either "normal" $REE_N$ patterns or LREE-enriched patterns. Garnet from phlogopite-garnet wehrlite exhibits the highest LREE-enrichment, with a maximum around the LREE-HREE limit and flat HREE. (3) Garnet macrocrysts with "normal" and "sinusoidal" $REE_N$ patterns [26]. Garnet macrocrysts from the TZ pipe exhibit both "normal" and "sinusoidal" $REE_N$

patterns with lower HREE abundances. In contrast, garnet from xenoliths (garnet-lherzolite and phlogopite-garnet wehrlite) and macrocrysts from the CU79 kimberlite follows the "normal" $REE_N$ pattern but with slightly depleted values than garnet from the CA pipe.

The data indicate that garnet lherzolite xenoliths found in the CA and CU79 kimberlites were under different equilibration conditions and different degrees of metasomatism. The xenoliths from the CA kimberlite may have been generated by refertilization of a previously depleted peridotite. The xenoliths from the CU79 kimberlite might be the result of a depleted source but with a very limited enrichment in LREE.

**Figure 9.** Chondrite-normalized REE diagrams for representative xenoliths and macrocrysts from the CA, TZ and CU79 kimberlites. The gray zone represents the "normal" garnet pattern according to McLean *et al*. [26].

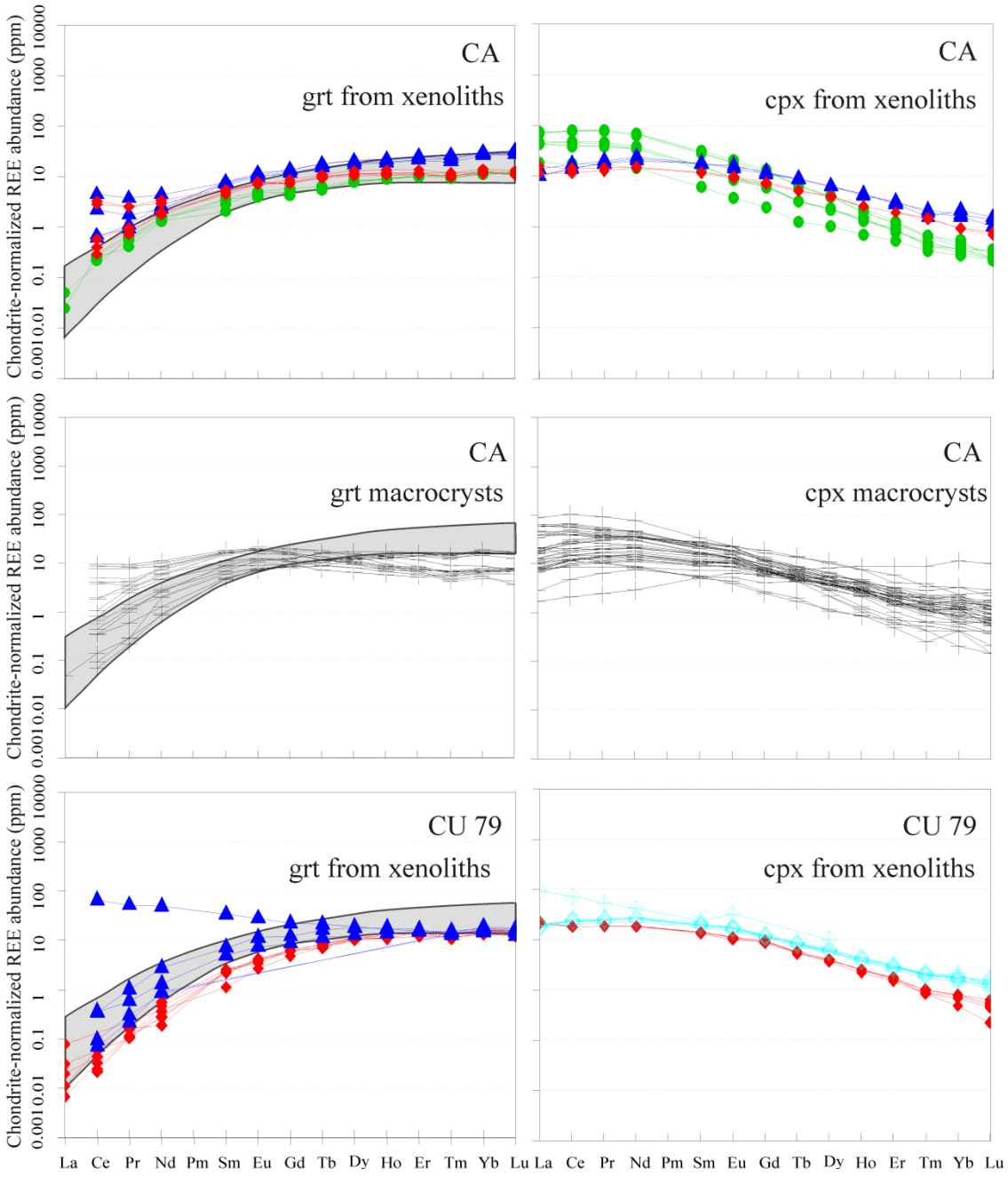

**Figure 9.** *Cont.*

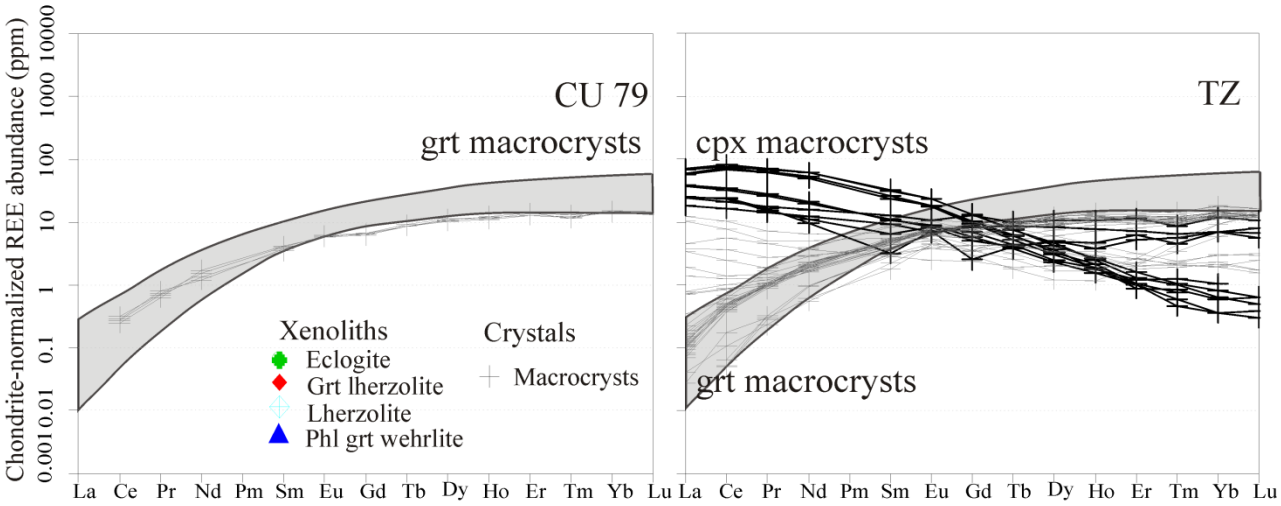


## 8. Sm/Nd Isotope Results for Xenoliths Whole-Rock

These data are the first Sm-Nd isotope analyses carried out in xenoliths of kimberlites from Angola (Table 5, supplementary file). Mantle xenoliths are potentially subject to infiltration and alteration of isotopic signatures from the kimberlite [27]. Consequently, it is important to mention that Sm-Nd model ages can reflect this mixing process. The mantle xenoliths from the CA kimberlite have a $^{143}Nd/^{144}Nd$ value between 0.511288 and 0.511681, whereas the Sm-Nd isotopes in xenoliths from the CU79 kimberlite show higher $^{143}Nd/^{144}Nd$ values between 0.512274 and 0.512391, as well as a narrower range of values. A single value of 0.512377 was obtained from the CU80 pipe, located 5.5 km SSE from the CU79 pipe, and can be used for comparison. Negative epsilon Nd ($\varepsilon_{Nd}$) values from xenoliths of the CA kimberlite indicate an enriched mantle, whereas mantle-derived xenoliths from the CU79 pipe show a slightly depleted mantle signature with positive $\varepsilon_{Nd}$ values as well as the sample from the CU80 pipe. The Nd isotope evolution diagram (Figure 10) clearly shows different sources for the two kimberlites (the CA and the CU79).

**Figure 10.** Diagram of $\varepsilon_{Nd}$ *vs.* T (Ga) for xenoliths from the CA, CU79, and CU80 kimberlites.

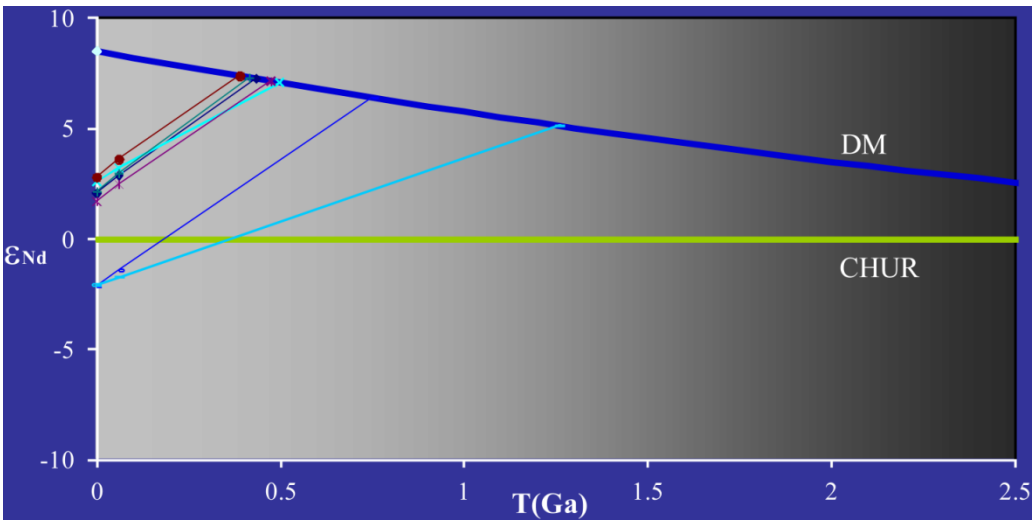

## 9. Discussion and Conclusions

### *9.1. Discrimination among Kimberlites*

The trans-lithosphere discontinuity of the Lucapa structure played a very important role by favoring a thermal perturbation, melt production, and mantle upwelling [28,29], and in the evolution of the host rocks. The integration of petrography, geochemistry, and geothermobarometric studies of the less altered samples from six kimberlites in the northeastern Angola suggests that these kimberlites originated from different sources in spite of the fact that they are all located in the same tectonic corridor.

The CA kimberlite has different compositional populations of olivine macrocrysts (homogeneous, "iddingsite" rimmed, and zoning olivine) which suggests different sources for those crystals, where they have likely been modified by subsequent crystallization. It is important to mention that heterogeneous crystallization is commonly found in volcanic rocks [30]. In the case of Catoca, Fe-Mg zoning in olivine indicates a state of disequilibrium that reflects the physical and chemical conditions that the mineral has experienced. This pipe is also characterized by the presence of pyrope and pyrope-almandine (G9 and G10 according to Grütter *et al.* [19,31]), a relative abundance of Cr-rich diopside, and the presence of eclogite, garnet lherzolite, carbonatite, and phlogopite-garnet wehrlite xenoliths. Orthopyroxene is less common than clinopyroxene in this pipe. Orthopyroxene is usually serpentinized. The very low amounts of orthopyroxene may be explained by rapid dissolution in the kimberlitic melt during transport [32]. Considering that clinopyroxene does not occur as a liquidus phase in Group I kimberlites, kimberlitic magma is the mechanism that brings mantle xenoliths to the surface. The clinopyroxene equilibrates at pressures greater than 30 kbar and the Cr:Na ratio in clinopyroxene from kimberlites usually is around 1. The solubility of kosmochlor ($NaCrSi_2O_6$) in diopside decreases with pressure and its limit of solubility may be at about 45 kbar [32], which suggests that the join jadeite ($NaAlSi_2O_6$)-kosmochlor is strongly influenced by pressure between 30 and 45 kbar. Then there is a difference in the Al-Na component in clinopyroxene from the CA pipe and the other studied kimberlites specially the CU79.

The samples from the An116, AC63 and AC4 pipes are so limited that conclusions regarding their origin and evolution should be taken with caution. It is clear that Cr-rich diopside is present in the An116 pipe, indicating a potential "deep" source. The garnet samples from the AC4 pipe suggest shallower pressure conditions, less than 20 kbar. In contrast, garnet from the AC63 pipe shows ranges of pressure between 20 and 43 kbar. The chemical composition of the AC4 garnet suggests crust-derived crystals, whereas garnet from xenoliths from the AC63 pipe suggests a mantle-derived source. Samples from the TZ pipe have some similarities with those from the CA pipe, but garnet from the TZ pipe is the only G9 type with different ranges of pressure (less than 43 kbar) and its clinopyroxene has a lower Cr content. Some of the T-P values from Catoca are consistent with data previously published by Aschepkov *et al*. [33] based on garnet and pyroxene xenocrysts.

### *9.2. The Underlying Mantle in the Northeastern Angola*

We propose that the Catoca kimberlite was generated from a depleted source. A subsequent metasomatic enrichment event (possibly more than one) incorporated incompatible LREE. Based on normalization to chondrite of REE concentrations in garnet and clinopyroxene, we can track the

behavior of these elements in the kimberlite. If garnet equilibrates with clinopyroxene, the result is to shift only LREE in garnet [34], as we observed in the "sinusoidal" pattern of garnet from phlogopite-garnet wehrlite xenoliths in the CA pipe. Garnet crystals from the TZ pipe show similar patterns as that of the CA pipe (*i.e.*, "normal" and "sinusoidal" $REE_N$ patterns). This also suggests a metasomatic enrichment of a previously depleted source.

In contrast, garnet from phlogopite-garnet wehrlite from the CU79 kimberlite shows "normal" $REE_N$ patterns. This suggests different degrees of enrichment, likely due to metasomatism. Garnet lherzolites from both kimberlites seem to be derived from a depleted mantle source.

Different Sm-Nd TD model ages from the CA and the CU79 pipes may also suggest different mantle sources or metasomatic events that modified the isotopic ratios in the mantle. TDM model ages from the CA kimberlite could indicate different time events than for the CU79 kimberlite. The differences in diamond production from the CA, TZ, CU79, and AC63 kimberlite pipes may be the result of different mantle sources and metasomatic events, as well as independent subsequent evolution of each kimberlite.

We interpret different sources for both kimberlites (the CA and CU79 pipes). These two kimberlites have heterogeneous mantle sources, the CA kimberlite is the more enriched of the two, possibly because of multiple metasomatic events that could explain the "sinusoidal" $REE_N$ patterns in garnet. Both kimberlitic mantle xenoliths also have different TDM (Model ages relative to CHUR): the CA kimberlite xenoliths show Mesoproterozoic ages (1220–1250 Ma), whereas the CU79 kimberlite xenoliths yield 450 to 390 Ma (Late Ordovician to Devonian) like the TDM from the CU80 kimberlite.

These model ages may be interpreted as the age of mantle generation or the age of a metasomatic event that modified the isotopic ratios in the mantle. TDM model ages of 1.2 Ga or the xenoliths from the CA kimberlite could be associated with the Kibaran orogeny, whereas the ages from the CU79 kimberlite could imply more juvenile Paleozoic components possibly related to the assembly of Pangea. Based on these data, these two kimberlites with different diamond production grades have a different pattern of evolution despite being from the same tectonic trend, the Lucapa structure.

The reactivation of old deep-seated faults during the Paleoproterozoic, the Permo-Triassic, the Cretaceous and the Cenozoic [29] probably is an important factor in some of the different pulses of diamondiferous kimberlites. Thus petrography, geochemistry and Sm-Nd isotopic data from these kimberlites provide interesting tools to recognize possible diamondiferous kimberlites in the area.

## Acknowledgements

This research is funded by the CGL2006-12973 and CGL2009-13758 BTE projects of Ministerio de Educación y Ciencia (Spain), and the AGAUR SGR 589 and SGR444 of the Generalitat de Catalunya. The first author (SERC) received an FI grant and a BE grant, both sponsored by the Departament d'Educació i Universitats de la Generalitat de Catalunya and the European Social Fund. We thank D.G. Pearson and a second anonymous reviewer for their revision of this manuscript and all their valuable comments. We acknowledge the Geological Survey of Canada (GSC), Ottawa, for all of the support during a six-month Volunteer Assistant visit of SERC, especially to S.E. Jackson who gave us all the support and guidance for carrying out the LA-ICP-MS analyses. SERC thanks T. Stachel for providing the PTEXL.XLT program and guidance in the application of the geothermobarometers.

SERC also thanks K.A. Mather who kindly helped her to calculate the Angola paleogeotherm. The authors also acknowledge the Electron Microprobe Laboratory, Department of Earth and Planetary Sciences, McGill University, especially to Lang Shi for assistance in the use of EPMA. The authors also thank Robert Martin, emeritus professor at the Earth & Planetary Sciences Department, McGill University, who kindly arranged everything to acquire the EPMA analyses at the McGill University and made valuable improvements to the preliminary version of this manuscript. Thanks to the Pacific Centre for Isotopic and Geochemical Research, Department of Earth and Ocean Sciences, University of British Columbia, Vancouver, especially to B. Kieffer for all his collaboration in the developing the Sm-Nd analyses. We thank ENDIAMA (Empresa Nacional de Diamantes de Angola), which kindly allowed SERC to acquire samples for her Ph.D. thesis and allowed the use of all facilities for the mine trip, especially to M. Watangua (former Chief Geologist) and V. Pervov (petrologist). Also thank to A. Gonçalves, professor at the Universidade Agostinho Neto, Angola, who helped in all the process of logistics and develop the field trip. The authors also thank the Serveis Cientificotècnics de la Universitat de Barcelona for assistance in the use of SEM/ESEM-BSE-EDS analyses (E. Prats. And J. Garcá Veigas).

## References

1. ENDIAMA–Empresa Nacional de Diamantes de Angola, E.P. The State Owned Company responsible for the exploration, research, mining, polishing, cutting and trading of Angolan diamonds. History. Available online: http://www.endiama.co.ao/endiama_historia.php# (accessed on 8 July 2012).
2. Reis, B. Preliminary note on the distribution and tectonic control of kimberlites in Angola. In *Proceedings of the 24th International Geological Congress*, Montreal, Canada, 21 August–1 September 1972; Volume 24, pp. 276–281.
3. The Israeli Diamond Industry. Diamond news. The Israeli Diamond Industry Portal Newsletter. Available online: http://www.israelidiamond.co.il/english/news.aspx?boneid=918&objid=9920 (accessed on 25 September 2011).
4. Mitchell, R.H. *Kimberlites, Orangeites, and Related Rocks*; Plenum Press: New York, NY, USA, 1995; p. 410.
5. Scott Smith, B.H.; Nowicki, T.E.; Russell, J.K.; Webb, K.J.; Mitchell, R.H.; Hetman, C.M.; Harder, M.; Skinner, E.M.W.; Robey, J.V. Kimberlite Terminology and Classification. In *Proceedings of the 10th Kimberlite Conference*, Bangalore, India, 6–11 February 2012; Abstract Volume, 10IKC-226.
6. De Carvalho, H.; Tassinari, C.; Alves, P.H. Geochronological review of the Precambrian in western Angola: Links with Brazil. *J. Afr. Earth Sci.* **2000**, *31*, 383–402.
7. Guiraud, R.; Bosworth, W.; Thierry, J.; Delplanque, A. Phanerozoic geological evolution of Northern and Central Africa: An overview. *J. Afr. Earth Sci.* **2005**, *43*, 83–143.
8. Perevalov, O.V.; Voinovsky, A.S.; Tselikovsky, A.F.; Agueev, Y.L.; Polskoi, F.R.; Khódirev, V.L.; Kondrátiev, A.I. *Geology of Angola: Explanatory Notes of the Geological Map at a Scale of 1:1.000.000*; Geological Survey of Angola: Luanda, Angola, 1992.

9. Egorov, K.N.; Roman'ko, E.F.; Podvysotsky, V.T.; Sablukov, S.M.; Garanin, V.K.; D'yakonov, D.B. New data on kimberlite magmatism in southwestern Angola. *Russ. Geol. Geophys.* **2007**, *48*, 323–336.
10. Robles-Cruz, S.E.; Escayola, M.; Jackson, S.; Galí, S.; Pervov, V.; Watangua, M.; Gonçalves, A.; Melgarejo, J.C. U-Pb SHRIMP geochronology of zircon from the Catoca kimberlite, Angola: Implications for diamond exploration. *Chem. Geol.* **2012**, *310–311*, 137–147.
11. Eley, R.; Grütter, H.; Louw, A.; Tunguno, C.; Twidale, J. Exploration Geology of the Luxinga kimberlite Cluster (Angola) with evidence supporting the presence of kimberlite lava. In *Proceedings of the 9th Kimberlite Conference*, Frankfurt, Germany, 10–15 August 2008; Abstract Volume, 9IKC-A-00166.
12. Weis, D.; Kieffer, B.; Maerschalk, C.; Barling, J.; de Jong, J.; Williams, G. A.; Hanano, D.; Pretorius, W.; Mattielli, N.; Scoates, J.S.; Goolaerts, A.; Friedman, R.M.; Mahoney, J.B. High-precision isotopic characterization of USGS reference materials by TIMS and MC-ICP-MS. *Geochem. Geophys. Geosyst.* **2006**, *7*, Q08006:1–Q08006:30.
13. Pervov, V.A.; Somov, S.V.; Korshunov, A.V.; Dulapchii, E.V.; Fédix, J.T. The Catoca kimberlite pipe, Republic of Angola: A paleovolcanological model. *Geol. Ore Deposits* **2011**, *53*, 295–308.
14. Robles-Cruz, S.; Watangua, M.; Melgarejo, J.C.; Galí, S. New insights into the concept of ilmenite as an indicator for diamond exploration, based on kimberlite petrographic analysis. *J. Span. Soc. Mineral. Macla* **2008**, *9*, 205–206.
15. Pettit, W. Geophysical signatures of some recently discovered large (>40 ha) kimberlite pipes on the Alto Cuilo concession in northeastern Angola. *Lithos* **2009**, *112*, S106–S115.
16. Robles-Cruz, S.; Watangua, M.; Isidoro, L.; Melgarejo, J.C.; Galí, S.; Olimpio, A. Contrasting compositions and textures of ilmenite in the Catoca kimberlite, Angola, and implications in exploration for diamond. *Lithos* **2009**, *112*, S966–S975.
17. Pearson, D.G.; Canil, D.; Shirey, S.B. Mantle Samples Included in Volcanic Rocks: Xenoliths and Diamonds. In *The Mantle and Core: Treatise on Geochemistry*; Carlson, R.W., Ed.; Elsevier Science: Amsterdam, The Netherlands, 2003; Volume 2, pp.171–275.
18. Pearson, D.G.; Wittig, N. Formation of Archean continental lithosphere and its diamonds: The root of the problem. *J. Geol. Soc.* **2008**, *165*, 895–914.
19. Grütter, H.S.; Gurney, J.J.; Menzies, A.H.; Winter, F. An updated classification scheme for mantle-derived garnet, for use by diamond explorers. *Lithos* **2004**, *77*, 841–857.
20. Morris, T.F.; Sage, R.P.; Ayer, J.A.; Crabtree, D.C. A study in clinopyroxene composition: Implications for kimberlite exploration. *Geochem. Explor. Environ. Anal.* **2002**, *2*, 321–331.
21. Ramsay, R.R. Geochemistry of Diamond Indicator Minerals. Ph.D. Thesis, University of Western Australia, Perth, Australia, 1992.
22. Stachel, T. University of Alberta, Edmonton, Alberta, Canada. EXCEL spreadsheet to do geothermobarometry for mantle assemblages: Developments up to date and recent calibrations in geothermobarometry of mantle rocks based on the PTEXL program written by Thomas Köhler in 1994. Unpublished work, 2011.
23. Nimis, P.; Taylor, W.R. Single clinopyroxene thermobarometry for garnet peridotites. Part I. Calibration and testing of a Cr-in-Cpx barometer and an enstatite-in-Cpx thermometer. *Contrib. Mineral. Petrol.* **2000**, *139*, 514–554.

24. Nimis, P. Evaluation of diamond potential from the composition of peridotitic chromian diopside. *Eur. J. Mineral.* **1998**, *10*, 505–519.
25. Mather, K.A.; Pearson, D.G.; McKenzie, D.; Kjarsgaard, B.; Priestley, K. Constraining the depth and thermal history of cratonic lithosphere using peridotite xenolith and xenocryst thermobarometry and seismology. *Lithos* **2011**, *125*, 729–742.
26. McLean, H.; Banas, A.; Creighton, S.; Whiteford, S.; Luth, R.W.; Stachel, T. Garnet xenocrysts from the Diavik mine, NWT, Canada: Composition, color, and paragenesis. *Can. Mineral.* **2007**, *45*, 1131–1145.
27. Pearson, D.G. The age of continental roots. *Lithos* **1999**, *48*, 171–194.
28. White, S.H.; de Boorder, H.; Smith, C.B. Structural controls of kimberlite and lamproite emplacement. *J. Geochem. Explor.* **1995**, *53*, 245–264.
29. Jelsma, H.; Barnett, W.; Richards, S.; Lister, G. Tectonic setting of kimberlites. *Lithos* **2009**, *112*, 155–165.
30. Brett, R.C.; Russell, J.K.; Moss, S. Origin of olivine in kimberlite: Phenocryst or impostor? *Lithos* **2009**, *112*, S201–S212.
31. Grütter, H.; Latti, D.; Menzies, A. Cr-saturation arrays in concentrate garnet compositions from kimberlite and their use in mantle barometry. *J. Petrol.* **2006**, *47*, 801–820.
32. Vredevoogd, J.J.; Forbes, W.C. The system diopside–ureyite at 20 kb. *Contrib. Mineral. Petrol.* **1975**, *52*, 147–156.
33. Aschepkov, I.V.; Rotman, A.Y.; Somov, S.V.; Afanasiev, V.P.; Downes, H.; Logvinova, A.M.; Nossyko, S.; Shimupi, J.; Palessky, S.V.; Khmelnikova, O.S.; Vladykin, N.V. Composition and thermal structure of the lithospheric mantle beneath kimberlite pipes from the Catoca cluster, Angola. *Tectonophysics* **2012**, *530–531*, 128–151.
34. Stachel, T.; Viljoen, K.S.; Brey, G.; Harris, J.W. Metasomatic processes in lherzolitic and harzburgitic domains of diamondiferous lithospheric mantle. *Earth Planet. Sci. Lett.* **1998**, *159*, 1–12.